THE JOURNAL OF PHYSICAL CHEMISTRY B

Article

pubs.acs.org/JPCB

Water Accommodation on Ice and Organic Surfaces: Insights from Environmental Molecular Beam Experiments

Xiangrui Kong,*[,†] Erik S. Thomson,[†] Panos Papagiannakopoulos,[†,‡] Sofia M. Johansson,[†] and Jan B. C. Pettersson*[,†]

[†]Department of Chemistry and Molecular Biology, Atmospheric Science, University of Gothenburg, SE-412 96 Gothenburg, Sweden

[‡]Department of Chemistry, Laboratory of Photochemistry and Kinetics, University of Crete, GR-71 003 Heraklion, Greece

Supporting Information

ABSTRACT: Water uptake on aerosol and cloud particles in the atmosphere modifies their chemistry and microphysics with important implications for climate on Earth. Here, we apply an environmental molecular beam (EMB) method to characterize water accommodation on ice and organic surfaces. The adsorption of surface-active compounds including short-chain alcohols, nitric acid, and acetic acid significantly affects accommodation of D_2O on ice. *n*-Hexanol and *n*-butanol adlayers reduce water uptake by facilitating rapid desorption and function as inefficient barriers for accommodation as well as desorption of water, while the effect of adsorbed methanol is small. Water accommodation is close to unity on nitric-acid- and acetic-acid-covered ice, and accommodation is significantly more efficient than that on the bare ice surface. Water uptake is inefficient on solid alcohols and acetic acid but strongly enhanced on liquid phases including a quasi-liquid layer on solid *n*-butanol. The EMB method provides unique information on accommodation and rapid kinetics on volatile surfaces, and these studies suggest that adsorbed organic and acidic compounds need to be taken into account when describing water at environmental interfaces.

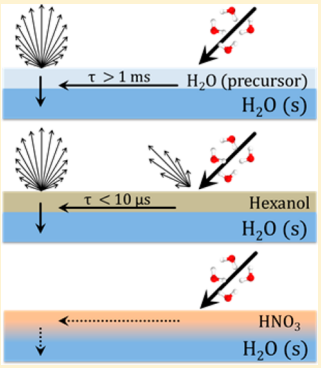

1. INTRODUCTION

Aerosols and clouds are of central importance for climate on Earth due to their effects on the chemistry and radiation budget of the atmosphere and on the transport of energy, water, and other components within the Earth system. Water exchange with aerosol and cloud particles modifies these environmental processes, which brings focus, even urgency, to the question of how molecular water interacts with condensed phases in the atmosphere. Water molecules undergo continuous condensation and evaporation on existing surfaces, with rates that depend on the detailed conditions at the interface. Even though the bulk properties of a condensed material may be well understood, surface properties are often distinctly different, a well-known example being the formation of a disordered surface layer on ice below the melting point.[1] In addition, insoluble or incompletely soluble compounds may concentrate at interfaces and thereby affect heterogeneous processes. Organic compounds are of particular interest due to their abundance and their intricate changes during slow oxidation in the atmosphere, which result in formation of secondary organic aerosols and coatings on existing particles.[2] The importance of water exchange with these and other surfaces calls for models with predictive power for the wealth of systems encountered in the environment. Although here we focus on systems of relevance for the atmosphere, we also emphasize that water interactions with condensed phases is not exclusively an environmental issue but is also of fundamental interest and importance to several other research fields.

Collisions between gas molecules and a surface typically result in trapping of molecules and surface accommodation within a few picoseconds.[3] The fraction of incoming molecules that trap is described by the surface accommodation coefficient α_s.[3] An alternative thermal accommodation coefficient α_t can be defined as the fraction of molecules that equilibrate to the surface temperature in all translational and internal degrees of freedom. For the systems studied here, thermal and surface accommodation take place on similar time scales and are indistinguishable with the employed experimental methods; hence, surface accommodation will be used throughout this study. Bulk accommodation α_b describes the more complex process whereby molecules are incorporated into the bulk of the condensed phase and is defined as the number of molecules incorporated into the particle bulk divided by the total number of molecules colliding with the surface.[3] The definition of α_b does not fundamentally require an accompanying time unit, but actual α_b values may vary depending on the absolute time scale considered. Bulk accommodation often takes place on a long time scale compared to surface accommodation. For example, water molecules will, on average, spend approximately 5 ms on an ice surface at 200 K before either desorbing or diffusing into the bulk.[4]

Special Issue: Physics and Chemistry of Ice 2014

Received: May 5, 2014
Revised: July 25, 2014
Published: July 31, 2014

Here, we focus on water accommodation on ice and organic surfaces that serve as proxies for the more complex systems expected to be found in the atmosphere. Several studies confirm that α_s for water molecules on ice is close to unity due to efficient energy transfer to phonons at surface impact and a relatively high binding energy for water to the ice surface.[5−8] The bulk accommodation coefficient for water on pure ice surfaces is much less well constrained. Earlier studies report α_b values that vary by more than 2 orders of magnitude,[9−27] with potential influence on the description of ice clouds in atmospheric models.[23,28,29] The situation is further complicated by effects of surface-active compounds that tend to concentrate at interfaces. This occurs when adsorbates condense directly from the gas phase or when ice grows and segregates foreign material from the crystal structure.[1] Atmospheric experiments and modeling suggest that uptake of common acids like HNO_3, HCl, and acetic acid (AcOH) may be substantial under typical cirrus cloud conditions,[30,31] and the resulting effects on water accommodation thus need to be considered.[14,32] Water interactions with organic phases are no better understood, and changes in hydrophilicity with oxidation state also need to be considered under atmospheric conditions.[2,33] To begin to address these questions, we have recently investigated the effect of adsorbed alcohols[34] and AcOH[32] on water uptake on ice, as well as water accommodation on the bulk phases of these compounds.[32,35]

Experimental tools for exploring microphysical and chemical processes taking place on volatile surfaces are limited. In addition to spectroscopic methods, a large number of techniques use ions, electrons, atoms, or molecules for surface analysis and process studies. The methods usually require high vacuum conditions because the finite vapor pressures over volatile surfaces may hinder transmission of probe particles to and from the surface. Among these surface-sensitive methods, molecular beam techniques play a central role for the development of a molecular-level understanding of reaction dynamics and kinetics of gas−solid interactions.[36] In the past few years, we have developed a molecular beam technique that allows for experiments at pressures up to 1 Pa, which makes it possible to perform experiments with ice and other volatile materials under conditions relevant for atmospheric processes.[4,7,32,34,35,37,38] The method has been termed an environmental molecular beam (EMB) method in analogy with environmental scanning electron microscopy (ESEM) that is carried out at elevated pressures.

Here, we present results from recent EMB studies with emphasis on water accommodation on ice and organic surfaces. The overall aim is to characterize the mechanisms that govern water uptake in order to guide the development of physics-based models to be used in atmospheric modeling. We present results for several new systems including *n*-hexanol (HxOH) adlayers on water ice, solid HxOH, two-dimensional (2D) HxOH films on a graphite surface, HNO_3−H_2O ice, and a HNO_3 monolayer on graphite. These new results are compared with previous EMB adsorbate studies. Taken as a whole, the suite of EMB studies can be used to contextualize the current understanding of atmospherically relevant water accommodation processes.

2. EXPERIMENTAL SECTION

A. Environmental Molecular Beam Method. The EMB method employed to study water−surface interactions has been described in detail elsewhere[37,38] but is briefly presented here to provide the experimental fundamentals. The EMB apparatus consists of a six-chamber high-vacuum system, and the main components are illustrated in Figure 1. A pulsed gas source is

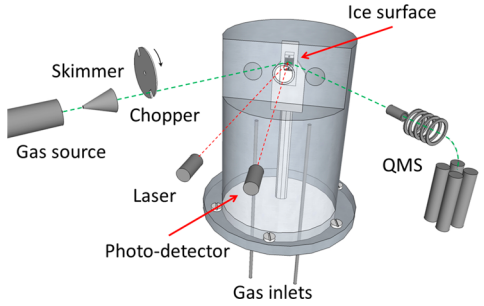

Figure 1. Schematic view of the EMB apparatus including the main components and the inner chamber surrounding the ice surface. The molecular beam and the direction of specular reflection are marked in green, and the direction of laser beam propagation is in red.

run with a D_2O/He mixture at a total pressure of 2×10^5 Pa and a partial D_2O pressure of approximately 2.2×10^3 Pa, which results in a molecular beam with mean kinetic energies of 31 ± 2 and 6.2 ± 0.3 kJ mol^{-1} for D_2O and He, respectively. A rotating chopper selects the central part of each gas pulse, and chopper frequencies of 8 and 120 Hz are used to produce long and short pulses depending on the time scale of interest in the experiments. The beam is directed toward a graphite surface (Advanced Ceramics Corp.; highly oriented pyrolytic graphite, grade ZYB, 12×12 mm^2) located in the center of the main ultrahigh vacuum (UHV) chamber. The UHV chamber has a background pressure of approximately 10^{-7} Pa that is primarily due to residual vapor from gases introduced during the experiments. The surface is enclosed by a separate inner chamber surrounding the surface, which allows for operation with vapor pressures up to approximately 1 Pa. The elevated pressures achieved within this system distinguish the method from traditional molecular beam experiments carried out under UHV conditions. The apparatus has been designed to minimize the molecular beam path length (28 mm) within the high-pressure zone, such that the attenuation of the beam due to gas collisions within the inner chamber becomes significant only above 10^{-1} Pa.[37] The incident beam collides with the surface at an angle of 45°, and the outgoing flux in the forward direction is monitored with a differentially pumped quadrupole mass spectrometer (QMS) at an angle of 45° from the surface-normal direction. The rotatable QMS is also used to measure in the incident beam.

Adsorbed layers are produced on the graphite substrate by introducing one or two high-purity gases into the environmental chamber through two separate gas inlets. Thick layers representing solid bulk phases of water and other compounds are formed by vapor deposition. A diode laser (0.86 mW, 670 nm) is used to monitor the thickness of adsorbed layers based on interference produced by reflections from the layer and the underlying substrate.[34,38] Layers are initially grown to a thickness of approximately 1 μm with typical growth rates of 1−60 monolayers s^{-1} depending on the system under investigation, and the pressure is then adjusted to maintain the layer at constant thickness. During the experiments, the investigated condensates are in a dynamic state characterized by rapid condensation and evaporation of the layer material. The typical uncertainty in layer thickness during the experiments is

dx.doi.org/10.1021/jp5044046 | J. Phys. Chem. B 2014, 118, 13378−13386

approximately 20 nm due to small deviations from steady-state conditions and the resolution of the interference measurements. Experiments are also carried out with adsorbed 2D phases on the graphite substrate, and the buildup and maintenance of monolayers on graphite are monitored by elastic helium scattering.[37,38] The graphite surface is cleaned between experiments by heating to 500 K, and clean surface conditions are routinely confirmed by elastic helium scattering after surface cooling to 200 K or lower. In experiments with adsorbed monolayers on ice, the surface coverage cannot be directly probed by helium scattering, and the experiments instead begin with the formation of a monolayer on graphite followed by the water inlet and growth of a thick ice layer while the trace gas inlet is kept constant. Monolayer coverage is experimentally verified by repeating experiments at different partial pressures following the procedure previously used to study alcohol and AcOH layers on ice.[32,34] In each case, the scattering results are unchanged, confirming complete HxOH coverage. The formation of a HxOH monolayer on ice is also consistent with existing isotherms in the literature.[39] During exploratory experiments with mixed HNO_3/H_2O ice, a partial HNO_3 pressure of 2×10^{-5} Pa is used and a nitric acid trihydrate (NAT) phase would form under equilibrium conditions,[40] but the detailed mixing ratio and structure in the bulk phase is likely to have been affected by the ice growth rate, and the formation of a crystalline NAT bulk phase has not been confirmed. The absolute HNO_3 pressure is estimated by comparison between the QMS signal for HNO_3 and the H_2O signal for a pure ice layer with a steady-state thickness, which is proportional to the equilibrium water pressure above ice.[32] The estimated uncertainty in absolute pressure is ±25% based on the typical agreement between literature values and observed QMS data for the present setup.

B. Data Analysis. In the experiments, short gas pulses first reach the surface, and the subsequent emissions from the surface are monitored using the QMS and recorded by a multichannel scaler with a 10 μs dwell time. Signals are typically integrated over time periods from minutes to several hours depending on the signal-to-noise ratio for the system under investigation. The following integration times are used in the present study: HxOH on graphite (10 min), solid HxOH (10 min), HxOH on ice (2 h), HNO_3 on graphite (30 min), and HNO_3 on ice (2 and 3 h). Typical resulting time-of-flight (TOF) distributions for D_2O interacting with three different HxOH-covered surfaces are illustrated in Figure 2. The TOF distributions are analyzed to determine probabilities for thermal desorption (TD) and inelastic scattering (IS), as well as desorption rate constants and the kinetic energy of scattered molecules. The distributions are described by the sum of two components corresponding to IS and trapping followed by TD. The IS distribution is assumed to have the form[41]

$$I_{IS}(v(t)) = C_1 v(t)^4 \exp\left[-\left(\frac{v(t) - \bar{v}}{v_{IS}}\right)^2\right] \quad (1)$$

where C_1 is a scaling factor, $v(t)$ is the velocity calculated from time t and the path length between the surface and the QMS, $\bar{v}$ represents the peak of the inelastically scattered velocities, and v_{IS} is

$$v_{IS} = \sqrt{\frac{2k_B T_{IS}}{m}} \quad (2)$$

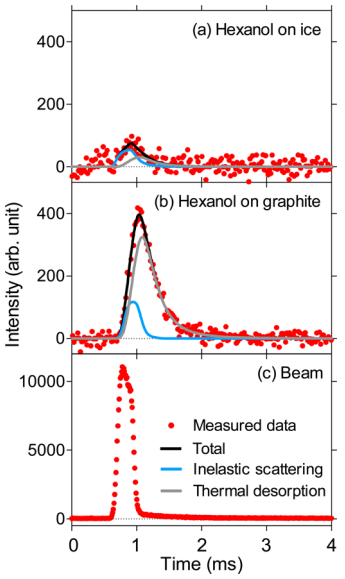

Figure 2. TOF distributions for D_2O IS and TD from (a) a HxOH monolayer on ice and (b) a HxOH monolayer on graphite. The time profile of the incident D_2O beam is shown in (c). The black, blue, and gray curves show the total, inelastic, and TD components, respectively, obtained from the nonlinear least-squares data fitting as described in the text. The experimental data have been normalized to the incident beam intensity and smoothed with a two-point stepwise average. The surface temperature was 190 K.

where T_{IS} describes the velocity spread, k_B is the Boltzmann constant, and m is the molecular mass. The TD component is modeled as an ordinary first-order desorption process and is expressed in terms of the measured intensity F as

$$F = C_2 e^{-kt} \quad (3)$$

where C_2 is a scaling factor and k is the desorption rate constant. The TOF distributions are fit in a nonlinear least-squares manner with C_1, C_2, k, T_{IS}, and $\bar{v}$ acting as free fitting parameters. The result is a convolution of the IS component, the TD component assuming that desorbing molecules have a thermal velocity distribution, and the D_2O flow to the ice surface described by the beam pulse profile.

The absolute TD probability, P_{TD}, is determined by normalizing the experimentally determined TD integral, I_{TD}, by the TD integral from a contiguously measured bare graphite case, $I_{TD}^{graphite}$.[34] The TD component has a cosine angular distribution,[42] and it is therefore sufficient to measure the intensity in one direction to determine the total emitted flux. Over the experimental temperature range, the TD probability for hyperthermal D_2O scattering from clean graphite is constant within the measurement uncertainty, and desorption from the bare graphite surface is linearly scaled by the sticking coefficient $s_{graphite} = 0.73 \pm 0.07$ for D_2O on bare graphite to obtain[34]

$$P_{TD} = \frac{s_{graphite} I_{TD}}{I_{TD}^{graphite}} \quad (4)$$

Error estimates for the integrated TD values are based on the 95% confidence intervals for the fitting parameters that describe the TD component, and final errors are based on propagating the error of each integral and the uncertainty in $s_{graphite}$.

For HxOH and HNO_3 on ice, a substantial fraction of the incoming D_2O molecules remain on the surface on the time

dx.doi.org/10.1021/jp5044046 | J. Phys. Chem. B 2014, 118, 13378−13386

scale of the experiment (10 or 60 ms), and we calculate an observed accommodation coefficient α_{obs} based on the absolute TD probability[32,34]

$$\alpha_{obs} = 1 - P_{TD} \quad (5)$$

Equation 5 ignores any losses of D_2O by IS, which is a valid assumption for HNO_3 on ice where no IS component is observed in the TOF distributions. In the case of HxOH on ice, an IS component is observed in the present hyperthermal experiments that favor IS compared to thermal collision energies. The absolute IS probability P_{IS} cannot be directly determined with the present system where the signal is measured at a single scattering angle. IS results in a directed flow in the forward direction,[5,6] and detailed knowledge about the angular distribution would be required to calculate P_{IS} from the experimentally determined IS integral. Although in the current experimental arrangement the IS and TD components often have comparable intensities due to the directed flow in the selected measurement direction, P_{IS} is typically less than a few percent of P_{TD} and is ignored in calculations of α_{obs} for HxOH-covered ice, in agreement with earlier studies of alcohol- and AcOH-covered ice.[32,34]

3. RESULTS AND DISCUSSION

A. Water Accommodation on Ice Surfaces. Here, we describe the effects of adsorbed HxOH and HNO_3 on water accommodation on ice and compare with recent EMB results for bare ice and ice covered with methanol (MeOH), *n*-butanol (BuOH), and AcOH. Figure 2a shows a TOF distribution for D_2O colliding with HxOH-covered ice at 190 K, overlaid by a two-component nonlinear least-squares fit of the data with each component (IS and TD) and the sum of the two components depicted. Comparable TOF results were obtained and analyzed for temperatures from 186 to 194 K. The IS peak is shifted in time relative to the incident beam (Figure 2c), and a final average kinetic energy of 6.1 ± 0.6 kJ mol^{-1} is calculated from the IS data, indicating that scattered water molecules lose approximately 80% of their kinetic energy in surface contact. The observed IS is due to the high incident kinetic energy used here, and IS is expected to be insignificant under thermal conditions due to efficient energy transfer to surface modes at impact.[5−8] The width of the TD distribution in Figure 2a is determined primarily by the thermal velocity distribution of desorbing D_2O, and the surface residence time of adsorbed water molecules is too short to be resolved (<20 μs). The observed TD probability is relatively low, and a major fraction of the incident water molecules remains on the surface on the time scale of the experiment. An accommodation coefficient of $\alpha_{obs} = 0.79 \pm 0.05$ is calculated using eqs 4 and 5. Recent EMB studies of D_2O interactions with BuOH-covered ice show comparable results with contributions from IS and rapid TD, while the emitted flux from a MeOH-covered ice surface is smaller and dominated by IS.[34]

The results for HxOH-covered ice are contrasted with corresponding data for D_2O interacting with a HxOH monolayer on graphite in Figure 2b. Alcohols are known to form monolayers with unique properties on graphite.[43,44] HxOH is no exception, and it is observed to form a stable monolayer, in agreement with similar results for MeOH and BuOH.[37,38] The TOF distribution for D_2O interacting with the HxOH/graphite system shows pronounced peaks for IS and TD. The IS intensity from a HxOH monolayer is higher than that from the HxOH/ice system, indicating qualitative differences in surface accommodation for the two systems. However, the final average kinetic energy in the HxOH monolayer system is identical to the HxOH-covered ice system, 6.1 ± 0.6 kJ mol^{-1}. Thus, the interaction with both HxOH-covered surfaces is characterized by efficient energy transfer. The TD component is considerably higher for D_2O on HxOH/graphite with $P_{TD} = 0.76 \pm 0.05$. In this case, D_2O has no ice phase into which it can escape, and the stable HxOH−HxOH bonds within the adlayer appear to preclude water from forming long-lasting hydrogen bonds, resulting in a surface with a hydrophobic character, in contrast to the HxOH/ice system.

Experiments were also carried out with ice surfaces covered with nitric acid. As previously outlined, NAT should form in equilibrium under the experimental conditions used here, but the detailed surface phase cannot be identified, and thus, we simply refer to it as HNO_3/H_2O or HNO_3-covered ice. Figure 3a illustrates that neither IS nor TD of D_2O is observed for a

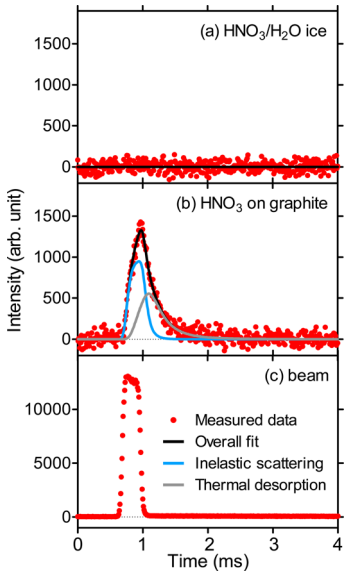

Figure 3. TOF distributions for D_2O IS and TD from (a) a HNO_3 layer on ice at 186 K and (b) a HNO_3 layer on graphite at 190 K. The time profile of the incident D_2O beam is shown in (c). The black, blue, and gray curves show the total, inelastic, and TD components, respectively, obtained from the nonlinear least-squares data fitting. The experimental data have been normalized to the incident beam intensity.

HNO_3-covered ice surface, and therefore, we conclude that HNO_3 adsorption has a strong effect on water accommodation compared to the alcohol-covered ices discussed above. A similar lack of TD is observed for D_2O on AcOH-covered ice, which however shows a small IS component.[34] Like HxOH, nitric acid is also found to form a stable monolayer on graphite, and we compare the ice and graphite systems in Figure 3. In contrast to HNO_3-covered ice, IS and TD of D_2O are substantial from HNO_3-covered graphite at 190 K (Figure 3b). Similar to the HxOH surfaces, gas−surface interactions are highly inelastic, with a final average kinetic energy of 6.2 ± 0.6 kJ mol^{-1}. Desorption dominates, with P_{TD} being close to unity because the surface does not provide strongly bound sites for water, in contrast to the hydrophilic HNO_3/H_2O ice.

Figure 4 displays the observed accommodation coefficients determined for each of the ice systems discussed above. The accommodation coefficient is around 0.8 on HxOH- and

dx.doi.org/10.1021/jp5044046 | J. Phys. Chem. B 2014, 118, 13378−13386

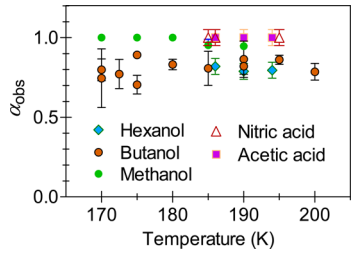

Figure 4. Water accommodation coefficient α_{obs} on ice coated with different adsorbates: HNO_3 (red △), HxOH (blue ◆), AcOH[32] (pink ■), BuOH[34] (orange ●), and MeOH[34] (green ●). All displayed data were computed from TD integrals determined on a 10 ms time scale in the experiments.

BuOH-covered ice with no clear temperature trend between 170 and 200 K. MeOH adlayers produce α_{obs} values close to unity, and the same is true for AcOH- and HNO_3-covered ice. The collected evidence thus demonstrates that adsorbed HNO_3, AcOH, and MeOH do not significantly hinder accommodation, while the larger alcohols HxOH and BuOH reduce water uptake to a small degree.

It is interesting to compare the present data with EMB results for D_2O accommodation on bare ice.[4] The D_2O−ice interactions are characterized by complete surface accommodation and bulk accommodation that decreases nonlinearly from close to unity at 170 K to 0.4 at 200 K. The accommodation data and desorption kinetics are well described by a precursor model where water molecules on average remain on the ice surface for tens of milliseconds before they either desorb or become incorporated in the ice structure.[4] The time scale for determination of α_b on bare ice was typically 60 ms,[4] while a shorter time scale would result in α values close to unity because of the slow desorption kinetics. The time scale for determination of α is thus important, and the 10 ms data shown in Figure 4 cannot be directly compared with the bare ice data.

To allow for a more detailed comparison, Figure 5 illustrates typical TOF distributions for D_2O emission from HxOH-

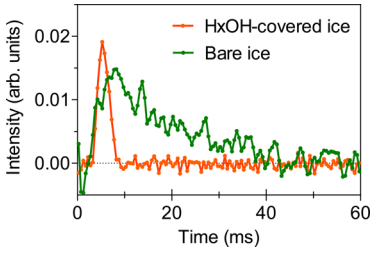

Figure 5. Comparison between 60 ms TOF distributions for D_2O IS and TD from a HxOH monolayer on ice (orange line) and from bare ice[4] (green line). The experimental data have been normalized to the incident beam intensity and smoothed with a 50 point stepwise average. The surface temperature was 190 K.

covered and bare ice measured on a 60 ms time scale. This makes plain that D_2O desorption from HxOH-covered ice only takes place during an initial phase, and no slow desorption component similar to the one seen for bare ice is observed. Likewise, no slow desorption is observed for HNO_3/H_2O ice (not shown) or for AcOH-covered ice.[32] To date, no corresponding 60 ms measurements have been carried out for MeOH- and BuOH-covered ice, but shorter time scale experiments show no indication of long decay processes.

Figure 6 summarizes the water accommodation coefficients determined for HxOH-, AcOH-, and HNO_3-coated ice surfaces

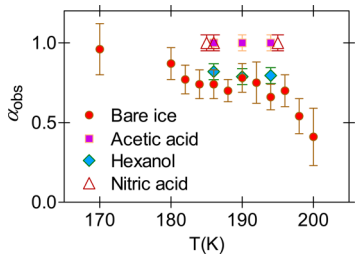

Figure 6. Water accommodation coefficient α_{obs} on ice determined from EMB experiments: HNO_3-covered ice (red △), HxOH-covered ice (blue ◆), AcOH-covered ice[32] (pink ■), and bare ice[4] (red ●). All displayed data were computed from TD integrals determined on a 60 ms time scale in the experiments.

together with the bare ice results.[4] Adsorption of nitric acid and AcOH results in α_{obs} values close to unity, and thus, the acids significantly enhance accommodation compared to pure ice. The observed α_{obs} values are comparable for HxOH-covered ice and bare ice, but as illustrated in Figure 5, the underlying kinetics are completely altered by the adsorption of the alcohol, which functions as a relatively inefficient barrier for accommodation as well as desorption of water.

In a related study, Davy and Somorjai used a vacuum microbalance technique and concluded that adsorbed NH_3 reduces and HF increases the ice evaporation rate, while adsorbed HCl had no observable effect.[14] Several earlier studies have also investigated the effects of alcohols on evaporation from liquid water surfaces. A monolayer of long alcohols with more than 12 carbon atoms reduces evaporation of liquid water, and the effect increases with increasing alkyl chain length.[45−47] Condensed films with long-range order efficiently suppress the evaporation coefficient, but islanding of adsorbed alcohols and changes in film structure due to temperature and composition may allow water to evaporate rapidly.[47] It remains to be shown whether the trends hold for short-chain alcohols. Gilde et al. performed MD simulations and reported that an adsorbed BuOH monolayer decreases water condensation on liquid water by a factor of 3 compared to bare water,[48] but Van Loon at el. concluded that BuOH and HxOH are not hydrophobic enough to form close-packed layers on top of liquid water, and they would thus have a limited effect on bulk accommodation.[49] Morita used MD simulations to study a liquid MeOH/water mixture and concluded that the accommodation coefficient is nearly unity.[50] Although the observations for liquid surfaces appear to qualitatively agree with our results for ice, the earlier work has limited predictive power for conditions on ice at 200 K and below. We conclude that new dedicated theoretical and experimental studies at temperatures that match the present experimental conditions will be required to provide a quantitative understanding of the accommodation process.

Water accommodation is no better understood on acid-covered surfaces. As noted for alcohol-covered surfaces, the effect of the adsorbate on water uptake may depend importantly on the structure of the covered ice surfaces. HNO_3 may dissociate on ice surfaces at low temperatures,[51−55] and the nitrates that are formed preferably concentrate at grain boundaries or at the vapor/ice interface.[56] Using ellipsometry, Moussa et al. found that the structure of ice surfaces can be

dx.doi.org/10.1021/jp5044046 | J. Phys. Chem. B 2014, 118, 13378−13386

more disordered when HNO_3 is present.[57] HNO_3 also forms hydrates with water,[58−60] which are likely to have different accommodation efficiencies than water ice. NAT coatings extend the lifetime of stratospheric ice particles,[61] and NAT has a lower equilibrium vapor pressure than ice,[62] which is consistent with our own observations. In the case of AcOH, the molecule binds relatively strongly to the ice surface, and uptake is found to be reversible.[39,63,64] However, the present understanding of the AcOH structure on ice is unclear, and views diverge with regard to the detailed structure and degree of protonation within the surface layer,[32] which makes it difficult to elucidate the detailed mechanism for accommodation of water.

The EMB studies shed new light on the water accommodation process on ice, and although it is premature to generalize, the existing data indicate that typical atmospheric adsorbates tend to increase rather than decrease water accommodation compared to pure ice. Under the present conditions, HxOH and BuOH are found to slightly reduce the accommodation coefficient by facilitating rapid desorption. However, at the same time, they induce changes in the ice layer properties and reduce the desorption rate for water molecules that have passed through the adsorbed layer. The experiments with nitric acid and AcOH suggest that they have an even more dramatic effect on water accommodation on ice, and in both cases, α_{obs} is significantly increased compared to pure ice. Additional HNO_3 accommodation experiments should be carried out that explore the phase diagram of the HNO_3/H_2O system. Progressive development of the EMB experiments to reach higher temperatures and vapor pressures should also be emphasized, together with complementary theoretical and experimental methods that describe the structure and diffusion processes in the near-surface region of the ice.

B. Water Accommodation on Organic Surfaces. A large fraction of the atmospheric aerosol consists of organic aerosol particles or inorganic particles with condensed organic components.[2] To begin to address water uptake on these surface, we have applied the EMB technique to a few model systems. Figure 7a shows a TOF distribution for D_2O colliding with a solid HxOH layer. The temperature is well below the 226 ± 6 K[65] melting point of HxOH, and the μm-thick layer is likely to be polycrystalline considering the high deposition rate in the experiments. The TOF distribution is well described by IS and an ordinary TD component. The average kinetic energy of the scattered molecules is 6.1 ± 0.6 kJ mol^{-1}, which is 80% of the incident kinetic energy. Thus, energy transfer is comparable to results for the previously described ice surfaces, and we conclude that surface accommodation can be expected to be close to unity under thermal conditions. The results also suggest that energy transfer is mainly determined by the detailed D_2O−HxOH molecular interactions during the brief surface encounters and less affected by differences in surface structure of the investigated HxOH-containing systems. The TD probability is substantially higher than that for HxOH-covered ice (Figure 2a) but comparable to the results for a HxOH layer on graphite (Figure 2b). We have observed a similar behavior for D_2O interactions with solid AcOH (P_{TD} = 0.71 ± 0.07),[32] and both HxOH and AcOH thus appear to have closed surface structures with limited opportunities for adsorbed water to form hydrogen bonds with surface molecules.

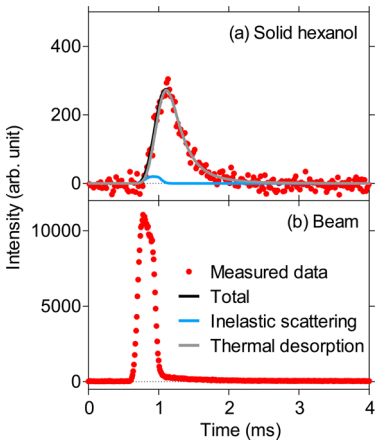

Figure 7. TOF distributions for D_2O IS and TD from a μm-thick solid HxOH layer. The lower panel shows the time profile for the incident D_2O beam. The black, blue, and gray curves show the total, inelastic, and TD components, respectively, obtained from the nonlinear least-squares data fitting as described in the text. The surface temperature was 190 K.

Considering the observed hydrophobic character of solid HxOH and knowing that HxOH is slightly soluble in water,[66] it would be interesting to study the effects of surface disorder and mobility as the temperature increases toward the melting point. Unfortunately, the present EMB setup does not allow for experiments at high enough temperatures and pressures to reach the melting point of HxOH(s). However, it is instructive to use recent results from MeOH and BuOH experiments for comparison.[7,35,37,38] MeOH has a high vapor pressure, and therefore, EMB experiments cannot be carried out with bulk MeOH. However, MeOH readily forms monolayers on graphite that can be used for detailed studies. MeOH monolayers on graphite have a low melting temperature of 135 K,[43] and water accommodation experiments have been carried out on this 2D liquid layer.[7] This is in contrast to HxOH, BuOH, and AcOH monolayers that all melt far above 200 K and result in water interactions of the type shown in Figure 2b (and discussed previously) over a wide temperature range. In the MeOH/graphite system, energy transfer between water molecules and the liquid layer is comparable to the previously mentioned solid surfaces,[7] but the TD kinetics are more interesting. Water molecules bind efficiently to the liquid MeOH layer, and a fraction remains accommodated on the adlayer over the 10 ms time scale of the experiments.[7] The desorption kinetics and accommodation data are qualitatively comparable to the bare ice results and might be better described by a two-state precursor model,[4] rather than being similar to the solid alcohol results.

Further evidence for the importance of surface conditions is given by experiments for the D_2O/BuOH system.[35] BuOH has a melting point of 184.5 K,[67,68] and water interactions with both solid and liquid BuOH have been studied with the EMB method.[35] Figure 8 shows calculated α_{obs} values as a function of temperature based on TD probability data reported in Papagiannakopoulos et al.[35] Below 180 K, the accommodation coefficient decreases with increasing temperature in a manner qualitatively similar to bulk accommodation on bare ice.[4] Above 180 K, α_{obs} rapidly increases as the temperature approaches and crosses the melting point. The observations have been attributed to surface melting of the BuOH crystal around 180 K and a thickening of the liquid-like layer as the melting temperature is approached.[35] Above the melting point, α_{obs} first

dx.doi.org/10.1021/jp5044046 | J. Phys. Chem. B 2014, 118, 13378−13386

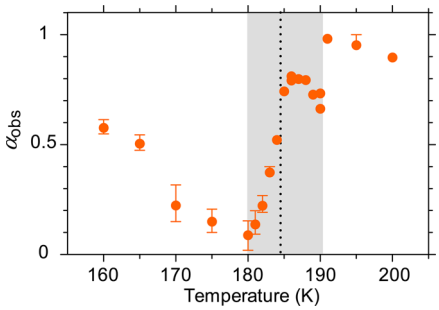

Figure 8. Water accommodation coefficient α_{obs} on BuOH calculated from the reported absolute TD probability data.[35] The dashed line indicates the melting temperature, and the gray marks the transition region where the surface properties of BuOH gradually change between solid and liquid.

levels out at around 0.7 and increases again above 190 K. The abrupt change at around 190 K suggests that the effect is caused by a phase transition rather than a gradual change due to increased temperature.[35] This could be explained by a phenomenon termed surface freezing, whereby straight-chain alcohols and alkanes have been found to undergo crystallization into bilayers above their melting points, at the surfaces of their liquids.[69−71] The surface of BuOH is not expected to form a solid crystalline bilayer, but the observed resistance to water uptake may be associated with a related ordering of the surface layer.[35] The intriguing results confirm the importance of liquid-like properties in the surface layer for accommodation of water, as also suggested by the MeOH/graphite data.

Clearly, water interactions with the organic systems discussed here sensitively depend on the state of the surface layer. The current studies should be seen as a starting point for systematic studies of molecular-level phenomena on organic surfaces. It has recently been suggested that secondary organic aerosols in the atmosphere may exist in a glassy intermediate state between solid and liquid over a wide temperature range,[72] and the importance of these conditions for water uptake and other heterogeneous processes remains to be determined. In the EMB experiments carried out to date, organic surfaces have been formed by vapor deposition, and further studies with more realistic organic phases such as di- and tricarboxylic acids will require new techniques for bringing less volatile substances into the high-vacuum environment.

4. CONCLUSIONS

We have carried out EMB studies with the aim of improving the understanding of water accommodation on ice and organic surfaces. Gas−surface collisions are highly inelastic in all studied systems and result in efficient surface accommodation of water molecules, which confirm the results from earlier molecular beam experiments.[5−8] In all cases, surface accommodation of water can safely be assumed to be close to unity on environmental surfaces under thermal conditions.

Water uptake on ice is found to be affected by the adsorption of surface-active compounds including short-chain alcohols, AcOH, and nitric acid. Adsorption of a HxOH layer facilitates rapid desorption of a small fraction of the trapped water molecules, but most molecules still reach the water ice structure. Thus, the alcohol layer functions as a rather inefficient barrier for accommodation and, at the same time, reduces the desorption rate for water. The results for BuOH layers on ice are comparable to the results for HxOH/ice, while the effect of adsorbed MeOH is small. Adsorption of nitric acid or AcOH increases α_{obs} to approximately unity and also reduces the water evaporation rate and therefore could have a major impact on the growth of ice cloud particles. Intriguingly, accommodation is significantly more efficient on the modified ice surfaces than that on pure bare ice. The governing mechanisms for the observed accommodation on the coated ice surfaces appear to be system-specific, although one general trend is that accommodation tends to increase rather than decrease with adsorption of compounds expected to be found in the atmosphere.

Bulk accommodation is inefficient on solid HxOH, and similar results are found for solid BuOH and AcOH. The condensed materials appear to produce hydrophobic surface structures, with limited opportunities for adsorbed water to form hydrogen bonds with surface molecules. The picture changes completely on liquid organic phases where water uptake is efficient in liquid MeOH monolayers on graphite and in liquid BuOH. The results for the D_2O/BuOH system are particularly intriguing, with substantial changes in water accommodation taking place over a 10 K interval below and above the BuOH melting point.

The EMB studies illustrate that adsorbed organic and acidic compounds may substantially modify the properties of environmental interfaces, with potential implications for the properties and action of aerosols and clouds in the Earth system. Further ice studies should focus on water uptake experiments with additional adsorbates of atmospheric relevance and also including mixed systems. Theoretical studies, including MD simulations, will also assist in the understanding of the detailed mechanisms behind bulk accommodation of water. Promising first results for organic surfaces should be built upon with systematic studies that explore the wealth of systems of relevance for environmental conditions. Continued development of the EMB technique also opens up new possibilities for detailed studies of reaction dynamics and kinetics in other types of volatile systems, with a large range of potential applications in science and technology. Further development of the EMB method is currently under way to allow for studies of gas−surface interactions at higher temperatures and pressures.

■ ASSOCIATED CONTENT

Ⓢ Supporting Information

Complete list of authors for refs 1−3, 25, 30, and 33. This material is available free of charge via the Internet at http://pubs.acs.org.

■ AUTHOR INFORMATION

Corresponding Authors

*E-mail: kongx@chem.gu.se. Tel. +46 31 7869071. Fax: +46 31 7721394 (X.K.).

*E-mail: janp@chem.gu.se. Tel. +46 31 7869072. Fax: +46 31 7721394 (J.B.C.P.).

Notes

The authors declare no competing financial interest.

■ ACKNOWLEDGMENTS

This work is supported by the Swedish Research Council and the Nordic Top-Level Research Initiative CRAICC. P.P. thanks the Wenner-Gren Foundation for providing funding for an extended stay at the University of Gothenburg.

REFERENCES

(1) Bartels-Rausch, T.; Bergeron, V.; Cartwright, J. H. E.; Escribano, R.; Finney, J. L.; Grothe, H.; Gutierrez, P. J.; Haapala, J.; Kuhs, W. F.; Pettersson, J. B. C.; et al. Ice Structures, Patterns, and Processes: A View across the Icefields. *Rev. Mod. Phys.* **2012**, *84*, 885−944.

(2) Hallquist, M.; Wenger, J. C.; Baltensperger, U.; Rudich, Y.; Simpson, D.; Claeys, M.; Dommen, J.; Donahue, N. M.; George, C.; Goldstein, A. H.; et al. The Formation, Properties and Impact of Secondary Organic Aerosol: Current and Emerging Issues. *Atmos. Chem. Phys.* **2009**, *9*, 5155−5236.

(3) Kolb, C. E.; Cox, R. A.; Abbatt, J. P. D.; Ammann, M.; Davis, E. J.; Donaldson, D. J.; Garrett, B. C.; George, C.; Griffiths, P. T.; Hanson, D. R.; et al. An Overview of Current Issues in the Uptake of Atmospheric Trace Gases by Aerosols and Clouds. *Atmos. Chem. Phys.* **2010**, *10*, 10561−10605.

(4) Kong, X.; Papagiannakopoulos, P.; Thomson, E. S.; Markovic, N.; Pettersson, J. B. C. Water Accommodation and Desorption Kinetics on Ice. *J. Chem. Phys. A* **2014**, *118*, 3973−3979.

(5) Andersson, P. U.; Någård, M. B.; Bolton, K.; Svanberg, M.; Pettersson, J. B. C. Dynamics of Argon Collisions with Water Ice: Molecular Beam Experiments and Molecular Dynamics Simulations. *J. Phys. Chem. A* **2000**, *104*, 2681−2688.

(6) Andersson, P. U.; Någård, M. B.; Pettersson, J. B. C. Molecular Beam Studies of HCl Interactions with Pure and HCl-Covered Ice Surfaces. *J. Phys. Chem. B* **2000**, *104*, 1596−1601.

(7) Thomson, E. S.; Kong, X. R.; Andersson, P. U.; Markovic, N.; Pettersson, J. B. C. Collision Dynamics and Solvation of Water Molecules in a Liquid Methanol Film. *J. Phys. Chem. Lett.* **2011**, *2*, 2174−2178.

(8) Gibson, K. D.; Killelea, D. R.; Yuan, H. Q.; Becker, J. S.; Sibener, S. J. Determination of the Sticking Coefficient and Scattering Dynamics of Water on Ice Using Molecular Beam Techniques. *J. Chem. Phys.* **2011**, *134*, 034703.

(9) Brown, D. E.; George, S. M.; Huang, C.; Wong, E. K. L.; Rider, K. B.; Smith, R. S.; Kay, B. D. H_2O Condensation Coefficient and Refractive Index for Vapor-Deposited Ice from Molecular Beam and Optical Interference Measurements. *J. Phys. Chem.* **1996**, *100*, 4988−4995.

(10) Bryson, C. E.; Cazcarra, V.; Levenson, L. L. Condensation Coefficient Measurements of H_2O, N_2O, and CO_2. *J. Vac. Sci. Technol.* **1974**, *11*, 411−416.

(11) Chaix, L.; Van den Bergh, H.; Rossi, M. J. Real-Time Kinetic Measurements of the Condensation and Evaporation of D_2O Molecules on Ice at 140 K < T < 220 K. *J. Phys. Chem. A* **1998**, *102*, 10300−10309.

(12) Chodes, N.; Warner, J.; Gagin, A. Determination of Condensation Coefficient of Water from Growth-Rate of Small Cloud Droplets. *J. Atmos. Sci.* **1974**, *31*, 1351−1357.

(13) Choularton, T. W.; Latham, J. Measurements of Deposition Coefficient for Ice, and Its Application to Cirrus Seeding. *Q. J. R. Meteorol. Soc.* **1977**, *103*, 307−318.

(14) Davy, J. G.; Somorjai, G. A. Studies of Vaporization Mechanism of Ice Single Crystals. *J. Chem. Phys.* **1971**, *55*, 3624−3636.

(15) Delval, C.; Flückiger, B.; Rossi, M. J. The Rate of Water Vapor Evaporation from Ice substrates in the Presence of HCl and HBr: Implications for the Lifetime of Atmospheric Ice Particles. *Atmos. Chem. Phys.* **2003**, *3*, 1131−1145.

(16) Delval, C.; Rossi, M. J. The Kinetics of Condensation and Evaporation of H_2O from Pure Ice in the Range 173−223 K: A Quartz Crystal Microbalance Study. *Phys. Chem. Chem. Phys.* **2004**, *6*, 4665−4676.

(17) Earle, M. E.; Kuhn, T.; Khalizov, A. F.; Sloan, J. Volume Nucleation Rates for Homogeneous Freezing in Supercooled Water Microdroplets: Results from a Combined Experimental and Modelling Approach. *Atmos. Chem. Phys.* **2010**, *10*, 7945−7961.

(18) Flückiger, B.; Rossi, M. J. Common Precursor Mechanism for the Heterogeneous Reaction of D_2O, HCl, HBr, and HOBr with Water Ice in the Range 170−230 K: Mass Accommodation Coefficients on ice. *J. Phys. Chem. A* **2003**, *107*, 4103−4115.

(19) Isono, K.; Iwai, K. Growth Mode of Ice Crystals in Air at Low Pressure. *Nature* **1969**, *223*, 1149−1150.

(20) Koros, R. M.; Deckers, J. M.; Andres, R. P.; Boudart, M. Sticking Probability of Water on Ice. *Chem. Eng. Sci.* **1966**, *21*, 941−950.

(21) Kramers, H.; Stemerding, S. The Sublimation of Ice in Vacuum. *Appl. Sci. Res., Sect. A* **1951**, *3*, 73−82.

(22) Leu, M. T. Laboratory Studies of Sticking Coefficients and Heterogeneous Reactions Important in the Antarctic Stratosphere. *Geophys. Res. Lett.* **1988**, *15*, 17−20.

(23) Magee, N.; Moyle, A. M.; Lamb, D. Experimental Determination of the Deposition Coefficient of Small Cirrus-Like Ice Crystals near −50°C. *Geophys. Res. Lett.* **2006**, *33*, L17813.

(24) Pratte, P.; Van den Bergh, H.; Rossi, M. J. The Kinetics of H_2O Vapor Condensation and Evaporation on Different Types of Ice in the Range 130−210 K. *J. Phys. Chem. A* **2006**, *110*, 3042−3058.

(25) Saunders, R. W.; Möhler, O.; Schnaiter, M.; Benz, S.; Wagner, R.; Saathoff, H.; Connolly, P. J.; Burgess, R.; Murray, B. J.; Gallagher, M.; et al. An Aerosol Chamber Investigation of the Heterogeneous Ice Nucleating Potential of Refractory Nanoparticles. *Atmos. Chem. Phys.* **2010**, *10*, 1227−1247.

(26) Skrotzki, J.; Connolly, P.; Schnaiter, M.; Saathoff, H.; Möhler, O.; Wagner, R.; Niemand, M.; Ebert, V.; Leisner, T. The Accommodation Coefficient of Water Molecules on Ice — Cirrus Cloud Studies at the AIDA Simulation Chamber. *Atmos. Chem. Phys.* **2013**, *13*, 4451−4466.

(27) Tolbert, M. A.; Middlebrook, A. M. Fourier-Transform Infrared Studies of Model Polar Stratospheric Cloud Surfaces — Growth and Evaporation of Ice and Nitric-Acid Ice. *J. Geophys. Res.* **1990**, *95*, 22423−22431.

(28) Gierens, K. M.; Monier, M.; Gayet, J. F. The Deposition Coefficient and Its Role for Cirrus Clouds. *J. Geophys. Res.* **2003**, *108*, 4069 DOI: 10.1029/2001JD001558.

(29) Lin, R. F.; Starr, D. O.; DeMott, P. J.; Cotton, R.; Sassen, K.; Jensen, E.; Karcher, B.; Liu, X. H. Cirrus Parcel Model Comparison Project. Phase 1: The Critical Components to Simulate Cirrus Initiation Explicitly. *J. Atmos. Sci.* **2002**, *59*, 2305−2329.

(30) Gao, R. S.; Popp, P. J.; Fahey, D. W.; Marcy, T. P.; Herman, R. L.; Weinstock, E. M.; Baumgardner, D. G.; Garrett, T. J.; Rosenlof, K. H.; Thompson, T. L.; et al. Evidence That Nitric Acid Increases Relative Humidity in Low-Temperature Cirrus Clouds. *Science* **2004**, *303*, 516.

(31) Marécal, V.; Pirre, M.; Rivière, E. D.; Pouvesle, N.; Crowley, J. N.; Freitas, S. R.; Longo, K. M. Modelling the Reversible Uptake of Chemical Species in the Gas Phase by Ice Particles Formed in a Convective Cloud. *Atmos. Chem. Phys.* **2010**, *10*, 4977−5000.

(32) Papagiannakopoulos, P.; Kong, X.; Thomson, E. S.; Pettersson, J. B. C. Water Interactions with Acetic Acid Layers on Ice and Graphite. *J. Chem. Phys. B* **2014**, DOI: 10.1021/jp503552w.

(33) Jimenez, J. L.; Canagaratna, M. R.; Donahue, N. M.; Prevot, A. S. H.; Zhang, Q.; Kroll, J. H.; DeCarlo, P. F.; Allan, J. D.; Coe, H.; Ng, N. L.; et al. Evolution of Organic Aerosols in the Atmosphere. *Science* **2009**, *326*, 1525−1529.

(34) Thomson, E. S.; Kong, X.; Markovic, N.; Papagiannakopoulos, P.; Pettersson, J. B. C. Collision Dynamics and Uptake of Water on Alcohol-Covered Ice. *Atmos. Chem. Phys.* **2013**, *13*, 2223−2233.

(35) Papagiannakopoulos, P.; Kong, X.; Thomson, E. S.; Markovic, N.; Pettersson, J. B. C. Surface Transformations and Water Uptake on Liquid and Solid Butanol near the Melting Temperature. *J. Chem. Phys. C* **2013**, *117*, 6678−6685.

(36) Scoles, G.; Bassi, D.; Buck, U.; Laine, D. C., Eds. *Atomic and Molecular Beam Methods*; Oxford University Press: New York, 1988.

(37) Kong, X.; Andersson, P. U.; Markovic, N.; Pettersson, J. B. C., *Environmental Molecular Beam Studies of Ice Surface Processes, Physics and Chemistry of Ice 2010*; Furukawa, Y., Sazaki, G., Uchida, T., Watanabe, N., Eds.; 12th International Conference on the Physics and Chemistry of Ice (PCI-2010); Hokkaido University Press: Sapporo, Japan, 2010; pp 79−88.

(38) Kong, X. R.; Andersson, P. U.; Thomson, E. S.; Pettersson, J. B. C. Ice Formation via Deposition Mode Nucleation on Bare and

Alcohol-Covered Graphite Surfaces. *J. Phys. Chem. C* **2012**, *116*, 8964−8974.
(39) Sokolov, O.; Abbatt, J. P. D. Adsorption to Ice of *n*-Alcohols (Ethanol to 1-Hexanol), Acetic Acid, and Hexanal. *J. Phys. Chem. A* **2002**, *106*, 775−782.
(40) Warshawsky, M. S.; Zondlo, M. A.; Tolbert, M. A. Impact of Nitric Acid on Ice Evaporation Rates. *Geophys. Res. Lett.* **1999**, *26*, 823−826.
(41) Buttner, R.; Maurer, G. Dimerisierung einiger organischer Sauren in der Gasphase. *Ber. Bunsen-Ges. Phys. Chem.* **1983**, *87*, 877−882.
(42) Marković, N.; Andersson, P. U.; Någård, M. B.; Pettersson, J. B. C. Scattering of Water from Graphite: Simulations and Experiments. *Chem. Phys.* **1999**, *247*, 413−430.
(43) Morishige, K.; Kawamura, K.; Kose, A. X-ray Diffraction Study of the Structure of a Monolayer Methanol Film Adsorbed on Graphite. *J. Chem. Phys.* **1990**, *93*, 5267−5270.
(44) Morishige, K.; Sakamoto, Y. Melting of *n*-Butanol and *n*-Pentanol Monolayers Adsorbed on Graphite: Effect of Molecular Length on Melting. *J. Chem. Phys.* **1995**, *103*, 2354−2360.
(45) La Mer, V. K.; Aylmore, L. A. G.; Healy, T. W. Ideal Surface Behavior of Mixed Monolayers of Long-Chain *n*-Paraffinic Alcohols. *J. Phys. Chem.* **1963**, *67*, 2793−2795.
(46) Barnes, G. T. Permeation through Monolayers. *Colloids Surf., A* **1997**, *126*, 149−158.
(47) Davies, J. F.; Miles, R. E. H.; Haddrell, A. E.; Reid, J. P. Influence of Organic Films on the Evaporation and Condensation of Water in Aerosol. *Proc. Natl. Acad. Sci. U.S.A.* **2013**, *110*, 8807−8812.
(48) Gilde, A.; Siladke, N.; Lawrence, C. P. Molecular Dynamics Simulations of Water Transport through Butanol Films. *J. Phys. Chem. A* **2009**, *113*, 8586−8590.
(49) Van Loon, L. L.; Minor, R. N.; Allen, H. C. Structure of Butanol and Hexanol at Aqueous, Ammonium Bisulfate, and Sulfuric Acid Solution Surfaces Investigated by Vibrational Sum Frequency Generation Spectroscopy. *J. Phys. Chem. A* **2007**, *111*, 7338−7346.
(50) Morita, A. Molecular Dynamics Study of Mass Accommodation of Methanol at Liquid−Vapor Interfaces of Methanol/Water Binary Solutions of Various Concentrations. *Chem. Phys. Lett.* **2003**, *375*, 1−8.
(51) Marchand, P.; Riou, S.; Ayotte, P. Diffusion Kinetics for Methanol in Polycrystalline Ice. *J. Phys. Chem. A* **2006**, *110*, 11654−11664.
(52) Krepelová, A.; Newberg, J. T.; Huthwelker, T.; Bluhm, H.; Ammann, M. The Nature of Nitrate at the Ice Surface Studied by XPS and NEXAFS. *Phys. Chem. Chem. Phys.* **2010**, *12*, 8870−8880.
(53) Riikonen, S.; Parkkinen, P.; Halonen, L.; Gerber, R. B. Ionization of Nitric Acid on Crystalline Ice: The Role of Defects and Collective Proton Movement. *J. Phys. Chem. Lett.* **2013**, *4*, 1850−1855.
(54) Pursell, C. J.; Everest, M. A.; Falgout, M. E.; Sanchez, D. D. Ionization of Nitric Acid on Ice. *J. Phys. Chem. A* **2002**, *106*, 7764−7768.
(55) Marcotte, G.; Ayotte, P.; Bendounan, A.; Sirotti, F.; Laffon, C.; Parent, P. Dissociative Adsorption of Nitric Acid at the Surface of Amorphous Solid Water Revealed by X-ray Absorption Spectroscopy. *J. Phys. Chem. Lett.* **2013**, *4*, 2643−2648.
(56) Wren, S. N.; Donaldson, D. J. Glancing-Angle Raman Study of Nitrate and Nitric Acid at the Air−Aqueous Interface. *Chem. Phys. Lett.* **2012**, *522*, 1−10.
(57) Moussa, S. G.; Kuo, M. H.; McNeill, V. F. Nitric Acid-Induced Surface Disordering on Ice. *Phys. Chem. Chem. Phys.* **2013**, *15*, 10989−10995.
(58) Hoyle, C. R.; Engel, I.; Luo, B. P.; Pitts, M. C.; Poole, L. R.; Grooss, J. U.; Peter, T. Heterogeneous Formation of Polar Stratospheric Clouds — Part 1: Nucleation of Nitric Acid Trihydrate (NAT). *Atmos. Chem. Phys.* **2013**, *13*, 9577−9595.
(59) Huthwelker, T.; Ammann, M.; Peter, T. The Uptake of Acidic Gases on Ice. *Chem. Rev.* **2006**, *106*, 1375−1444.
(60) Abbatt, J. P. D. Interaction of HNO_3 with Water−Ice Surfaces at Temperatures of the Free Troposphere. *Geophys. Res. Lett.* **1997**, *24*, 1479−1482.
(61) Biermann, U. M.; Crowley, J. N.; Huthwelker, T.; Moortgat, G. K.; Crutzen, P. J.; Peter, T. FTIR Studies on Lifetime Prolongation of Stratospheric Ice Particles due to NAT Coating. *Geophys. Res. Lett.* **1988**, *25*, 3939−3942.
(62) Hanson, D.; Mauersberger, K. Solubility and Equilibrium Vapor Pressures of HCl Dissolved in Polar Stratospheric Cloud Materials: Ice and the Trihydrate of Nitric Acid. *Geophys. Res. Lett.* **1988**, *15*, 1507−1510.
(63) Picaud, S.; Hoang, P. N. M.; Peybernès, N.; Le Calvé, S. Mirabel, P. Adsorption of Acetic Acid on Ice: Experiments and Molecular Dynamics Simulations. *J. Chem. Phys.* **2005**, *122*, 194707 DOI: 10.1063/1.1888368.
(64) von Hessberg, P.; Pouvesle, N.; Winkler, A. K.; Schuster, G.; Crowley, J. N. Interaction of Formic and Acetic Acid with Ice Surfaces between 187 and 227 K. Investigation of Single Species- and Competitive Adsorption. *Phys. Chem. Chem. Phys.* **2008**, *10*, 2345−2355.
(65) Afeefy, H. Y.; Liebman, J. F.; Stein, S. E. Neutral Thermochemical Data. In *NIST Chemistry WebBook*, NIST Standard Reference Database Number 69; Linstrom, P. J., Mallard, W. G., Eds.; National Institute of Standards and Technology: Gaithersburg, MD; http://webbook.nist.gov (retrieved May 4, 2014).
(66) Yaws, C. L.; Yang, H. C. Henry's Law Constant for Compound in Water. In *Thermodynamic and Physical Property Data*; Yaws, C. L., Ed.; Gulf Publishing Company: Houston, TX, 1992; pp 181−206.
(67) Wilhoit, R. C.; Chao, J.; Hall, K. R. Thermodynamic Properties of Key Organic Oxygen Compounds in the Carbon Range C-1 to C-4. Part 1. Properties of Condensed Phases. *J. Phys. Chem. Ref. Data* **1985**, *14*, 1−175.
(68) Haynes, W. M. Physical Constants of Organic Compounds. In *CRC Handbook of Chemistry and Physics*, 92nd ed., (Internet Version 2012) [Online]; CRC Press/Taylor and Francis: Boca Raton, FL, 2012.
(69) Gang, O.; Wu, X. Z.; Ocko, B. M.; Sirota, E. B.; Deutsch, M. Surface Freezing in Chain Molecules. II. Neat and Hydrated Alcohols. *Phys. Rev. E* **1998**, *58*, 6086−6100.
(70) Ocko, B. M.; Wu, X. Z.; Sirota, E. B.; Sinha, S. K.; Gang, O.; Deutsch, M. Surface Freezing in Chain Molecules: Normal Alkanes. *Phys. Rev. E* **1997**, *55*, 3164−3182.
(71) Sloutskin, E.; Bain, C. D.; Ocko, B. M.; Deutsch, M. Surface Freezing of Chain Molecules at the Liquid−Liquid and Liquid−Air Interfaces. *Faraday Discuss.* **2005**, *129*, 339−352.
(72) Virtanen, A.; Joutsensaari, J.; Koop, T.; Kannosto, J.; Yli-Pirila, P.; Leskinen, J.; Makela, J. M.; Holopainen, J. K.; Poschl, U.; Kulmala, M.; Worsnop, D. R.; Laaksonen, A. An Amorphous Solid State of Biogenic Secondary Organic Aerosol Particles. *Nature* **2010**, *467*, 824−827.